tvst

Article

Long-Term Effects of a Photodisruptive Laser-Induced Traumatic Neuropathy Model

Xiaoli Xing[1,2,*], Xiaowei Tong[1,3,*], Yuan Liu[1], Mary Tapia[1], Peiyao Jin[1,4], Timothy D. Holley[1,5], Oscar Qiu[1], and Richard K. Lee[1]

[1] Bascom Palmer Eye Institute, University of Miami Miller School of Medicine, Miami, FL, USA
[2] Tianjin Key Laboratory of Retinal Functions and Diseases, Tianjin International Joint Research and Development Centre of Ophthalmology and Vision Science, Eye Institute and School of Optometry, Tianjin Medical University Eye Hospital, Tianjin, China
[3] Shanghai Eye Diseases Prevention & Treatment Center, Shanghai Eye Hospital, National Clinical Research Center for Eye Diseases, Shanghai Key Laboratory of Ocular Fundus Diseases, Shanghai General Hospital, Shanghai, Shanghai Engineering Center for Visual Science and Photomedicine, Shanghai, China
[4] Department of Ophthalmology, Shanghai General Hospital, Shanghai Jiao Tong University School of Medicine, Shanghai, China
[5] Department of Ophthalmology, Virginia Commonwealth University, Richmond, VA, USA

Correspondence: Richard K. Lee, Walter G. Ross Distinguished Chair in Ophthalmology, Associate Professor of Ophthalmology, Cell Biology, and Neuroscience Graduate Program, Bascom Palmer Eye Institute, 900 NW 17th Street, Miami, FL 33136, USA.
e-mail: rlee@med.miami.edu

Received: June 13, 2020
Accepted: March 22, 2021
Published: July 12, 2021

Keywords: Nd:YAG laser; retinal ganglion cell; traumatic optic neuropathy; new model

Citation: Xing X, Tong X, Liu Y, Tapia M, Jin P, Holley TD, Qiu O, Lee RK. Long-term effects of a photodisruptive laser-induced traumatic neuropathy model. Transl Vis Sci Technol. 2021;10(8):8, https://doi.org/10.1167/tvst.10.8.8

Purpose: To create a mouse traumatic optic neuropathy (TON) model that is reproducible, reliable, and easy to manipulate with high specificity to retinal ganglion cell (RGC) layer and no mortality. The model will be useful for understanding the pathophysiology of retinal ganglion cell death and for testing neuroprotective therapeutics.

Methods: An Nd:YAG laser was used to generate focal photodisruptive retinal damage. Noninvasive in vivo ophthalmologic imaging technologies such as optical coherence tomography (OCT) and confocal laser scanning ophthalmoscopy (CSLO) were used to longitudinally track the retinal nerve fiber layer (RNFL) thickness and RGC number change, respectively. Immunostaining and pattern electroretinography (PERG) were also used to evaluate structure and functional change after laser injury.

Results: Our ND:YAG laser generates a concussive photodisruptive laser shockwave force which induces focal RGC death in the targeted area. We observed a correlative decrease in RGCs number, RNFL, and PERG function of RGC in the laser zone. The pattern of RNFL thinning and RGC soma loss correlates with the pattern and amount of fluorescence loss on OCT and CSLO images, respectively. The ND:YAG laser does not cause any damage to other layers in the retina nor any side effects including changes in intraocular pressure, corneal edema, and calcification or mortality (which has been observed in other TON models).

Conclusions: We have created a new and novel RGC TON death model that confers no mortality and produces a quantifiable decrease in RGC number and function. The laser targeted regions of the retina correlate with both in vivo imaging by OCT and CSLO and histologically with regions of RGC loss without ophthalmic side effects.

Translational Relevance: This laser-based TON injury model is simple to implement, is reproducible, and is useful for determining the molecular and cellular pathophysiology of TON and RGC death and for testing neuroprotective therapeutics.

Introduction

Traumatic optic neuropathy (TON) is a condition in which permanent vision loss is caused by blunt force trauma to the head or eye. It is uncommon but devastating. Traumatic injury is a key prognostic indicator usually associated with poor visual outcomes.[1] Activities associated with ocular trauma include sports injuries, work, falls, war injuries, and vehicle accidents.[2–4] Blunt ocular trauma is often worse than penetrating injury because blunt trauma typically causes transmural pressure waves, which run throughout the eye, causing widespread

shearing damage.[5] Furthermore, the blood-retinal barrier is often compromised.[6] In contrast, sharp penetrating trauma often results in focal injury over a smaller well-delineated region.

Several animal models of ocular trauma mimic specific mechanisms of injury and ocular disease observed in humans and can be used to develop potential treatments. Notable examples include weight drop injury; blast device injury, such as occurs with paintball gun blasting devices[7]; air tank blast injury[8]; and force percussion injury[9] and focal injury induced by ultrasound waves.[10] Although many of the models used have been shown to be useful for studying retinal injury, many are associated with significant side effects and even mortality, which is not typically observed in human patients suffering limited ocular trauma.[8]

The neodymium-doped yttrium aluminum garnet (Nd:YAG) laser to focus photo ablative laser injury onto the mouse retina. The Nd:YAG laser emits a wavelength 1064 nm energy and is widely used clinically. In patients with posterior capsular opacity, the YAG laser is used to safely ablate posterior capsular lens opacities. Moreover, in patients with narrow-angle or angle-closure glaucoma, the Nd:YAG laser is used to create a peripheral iridotomy to relieve elevated intraocular pressure (IOP) by creating an alternate pathway for aqueous humor outflow in the eye. The Nd:YAG laser can also be used to incise a variety of intraocular fibrotic tissues and tissue adhesions. The Nd:YAG laser produces a cloud of photodisruptive laser energy that acts in a wave-like pattern that is similar to localized blunt force trauma.

We have developed a novel retinal injury animal model, which is reproducible and more closely mimics the structural damage observed with traumatic optic neuropathy.[11] Using the Nd:YAG laser, we were able to induce localized damage to murine RGCs. Laser treated murine eyes were not exposed to any other source of injury, and control eyes were unaffected. Our purpose was to mimic the injuries causing by blunt trauma caused by objects such as airbags in vehicle crash, paintballs, bomb exposure in war, and other similar traumatic injuries.

Materials and Methods

Animals

All use of animals conformed with the Association for Research in Vision and Ophthalmology (ARVO) Statement for the Use of Animals in Ophthalmic and Vision Research and was approved by the Institutional Animal Care and Use Committee (IACUC) and the Institutional Biosafety Committee of the University of Miami.

In total, 45 three-month-old transgenic mice expressing channel rhodopsin-2 (ChR2) and enhanced yellow fluorescent protein (eYFP) under the retinal ganglion cell (RGC)–specific thymus cell antigen 1 (Thy1) promoter (Jackson Laboratory, Bar Harbor, ME) were used in this study.

Nd:YAG Laser Injury

An Nd:YAG laser generator (Lumenis Aura; Ophthalmic Lumenis Inc, Santa Clara, CA, USA) mounted on a slit lamp biomicroscope (Axioshop operating microscope; Carl Zeiss Meditec, Jena, Germany) was used in creating retinal injury. All animals will be anesthetized using a cocktail of Ketamine/Xylazine 90 to 100 mg/5 to 10 mg/kg via intraperitoneal injection. Anesthetized mice were mounted on a platform, and a glass coverslip with 2.5% hypromellose solution (Goniotaire; Altaire Pharmaceuticals, Aquebogue, NY, USA) was placed on the top of the cornea to allow visualization to the posterior pole of the eye. Nd:YAG laser with 0.4 mJ energy was focused on the vitreous anterior to the retina. The laser focus plane was first set at large vessels and moved anteriorly so that large vessels and the optic nerve head were avoided to minimize the risk bleeding from breaking of blood vessels by the laser. Two laser shots were taken in the peripapillary region circumferentially, and the average size of laser spot is 0.25 mm^2. The study left eye was injured by the Nd:YAG laser, with the opposite eye serving as a noninjured control eye.

Intraocular Pressure Measurements

A Tonolab rebound tonometer (TioLat, Helsinki, Finland) was used to measure the IOP of the study eyes, at baseline, 15 minutes after injury, one day and seven days after the injury. All IOP measures were performed in anesthetized mice. For each IOP recorded, six consequent IOP measurements were performed, and the mean value was used for statistical analysis.

Spectral Domain Optical Coherence Tomography (SD-OCT) Imaging and Segmentation

An SD-OCT customized for the murine eye (Bioptigen, Durham, NC, USA) was used to measure the cross-sectional structure of the retina. The axial

resolution of the OCT was 5 µm. The OCT was centered on the optic disc and then used a raster scan technique with a scan depth of 1000 × 100 (horizontal × vertical) and a coverage area of 1 × 1 mm^2 of mouse retina. The OCT scan covers all the quadrant and the laser area.

RNFL thickness is a surrogate marker for RGC axonal density.[12,13] The decrease of RNFL thickness indicated the loss of RGC. The thickness of nerve fiber layer was quantified as we have previously published.[14,15] Retinal thickness heat maps were generated from the retinal thickness measurements using a custom Matlab (Matlab R2015a; Natick, MA, USA)–based segmentation software to analyze the thickness changes of the retinal layers after Nd:YAG laser injury.

Confocal Scanning Laser Ophthalmoscopy (CSLO) Imaging

A customized Heidelberg Engineering CSLO (HRA II; Heidelberg Engineering, Heidelberg, Germany) was used to image Thy1-ChR2-eYFP RGCs in the mouse retina. Images were obtained in the red-free mode, and at the wavelength for green fluorescence (488 nm) with a rate of 51 frames per second. The scan range was 55°, and the angle of the scope to the retina changed to allow imaging of the peripheral retina in all quadrants of the eye.

Fundus fluorescein angiography and direct visualization was applied to confirm the source of hypo-fluorescence on CSLO images was truly the loss of RGCs, rather than obstructions such as vitreous hemorrhage. 0.03 mL of 10% fluorescein (Fluorescite; Alcon Laboratories, Fort Worth, TX, USA) was injected intraperitoneally into the mouse, and CSLO images were taken two minutes after the injection.

Tissue Collection

Mice were sacrificed 20 weeks after the laser treatment. Mice were then perfused transcardially using 4% paraformaldehyde in phosphate buffered saline solution (PBS) at a rate of 10 mL/min. The globes were enucleated with the 12 o'clock position marked, and then post-fixed with 4% paraformaldehyde/PBS overnight. After fixation, globes sent for cross-sectioning were embedded in paraffin, sectioned into 5 mm slices, and mounted onto glass slides. For whole mount samples, the retina was dissected before staining and mounting.

Immunofluorescence and Hematoxylin and Eosin Staining

For cross-sectional samples, after deparaffinization, sections were stained with hematoxylin and eosin to assess the structure of the surrounding retina. Slides for immunofluorescence staining were blocked with rodent blocker M (BioCare Medical, Concord, CA, USA) for 20 minutes at room temperature to minimize nonspecific antibody cross-reactivity. Primary antibodies were applied in 0.5% Triton (IB07100; Shelton Scientific, Shelton, CT, USA)/ PBS overnight at 4°C. After PBS washes, sections were then incubated with the secondary antibodies for two hours at room temperature. Finally, the stained sample was mounted onto a glass coverslip using 4′-diamidino-2-phenylindole dye (DAPI Vector, Burlingame, CA, USA) to label nuclei.

For preparation of whole mount retinal tissues, the isolated retina was blocked with rodent blocker M (BioCare Medical, Concord, CA, USA) for one hour at room temperature and then incubated with primary antibodies in 0.5% Triton/PBS for 48 hours at 4°C. After PBS washes, the retina was incubated with secondary antibodies for 24 hours at 4°C. Finally, the retina sample was mounted with DAPI (VectaShield; Vector, Burlingame, CA, USA) on charged glass slides.

The same primary and secondary antibodies were used in the immunofluorescence staining of cross-sectional samples and retinal whole mounts. The primary antibodies were goat anti-green fluorescent protein (GFP; 1:200; Rockland Immunochemicals, Gilbertsville, PA, USA) and rabbit anti-Brn3 (1:200; Santa Cruz Biotechnology, Santa Cruz, CA, USA). The secondary antibodies were, respectively, Alex Fluor 488 donkey anti-goat (1:500; Jackson Immuno Research Laboratories, West Grove, PA, USA) and donkey anti goat Cy5 (1:500, Jackson Immuno Research Laboratories). Stained retinal cross sections and retinal whole mounts were visualized with a confocal microscope (Leica TCS SP5 Confocal Microscope; Leica Microsystems, Buffalo Grove, IL, USA).

Pattern Electroretinography (PERG) and Flush Electroretinography Recording

During PERG recording, mice anesthetized with intra-peritoneal ketamine/xylazine were placed on a feedback-controlled heating pad (TCAT-2LV; Physitemp Instruments, Inc., Clifton, NJ, USA) to maintain constant body temperature at 37°C. For PERG recording, a semicircular silver loop electrode was placed on the topically anesthetized cornea.

Reference and ground electrodes were placed subcutaneously on the back of the head and the base of the tail, respectively. Anesthetized mice received a stimulus of contrast bars (field area, 69.4° × 63.4°; mean luminance, 50 cd/m2; spatial frequency, 0.05 cycles/deg; contrast, 98%; temporal frequency, 1 HZ) at 20 cm. Three independent test trials composed of 300 measurements was recorded for each eye, and the data were processed using Sigmaplot (version 11.2; Systat Software, Inc., San Jose, CA, USA). The peak to trough amplitude in a time window of 50 to 300 ms was automatically measured and analyzed by the software. Human bias and recording noise were excluded by a software algorithm. Corresponding measurement of control outer retinal function (light adapted flash ERG) were also recorded. Mice were placed on the same recording machine as for PERG testing and received strobe light flashes of 20 cd/m^2/s superimposed on a steady background light of 12 cd/m^2 presented within a Ganzfeld bowl. Control flash ERG for retinal function was evaluated with the same technique as the PERG.[16]

Statistical Analysis

SAS (version 8.0; SAS Institute, Cary, NC, USA) was used in statistical analyses. The characteristics were presented as the means ± standard deviation for continuous variables, and as rates (proportions) for categorical data. The data distribution was examined using Kolmogorov–Smirnov test. Repeated analysis of variance was used to compare the IOP, RNFL thickness, PERG amplitude and PERG latency measured in different time points in both groups. *T*-testing was used to compare the thickness between the study eyes and the control eyes. Statistical significance was defined as $P < 0.05$ (two-tailed).

Results

Nd:YAG Laser Generates Localized Injury With Few Side Effects

Immediately after the Nd:YAG laser treatment to the retina, a small air bubble was observed in the center of the aimed vitreous, and the laser cavitation bubble faded within five seconds. Temporary bleeding of microvessels was occasionally observed on the surface of retina around the blast, seen as a circle with margins exhibiting rubor—probably from photodisruptive laser force shearing small retinal vessels. SD-OCT retinal imaging demonstrates retinal edema and subretinal fluid locally in the laser injury region one week after the injury (Fig. 1B); both the retinal edema and subretinal fluid regressed after one to two weeks (Figs. 1B, 1C).

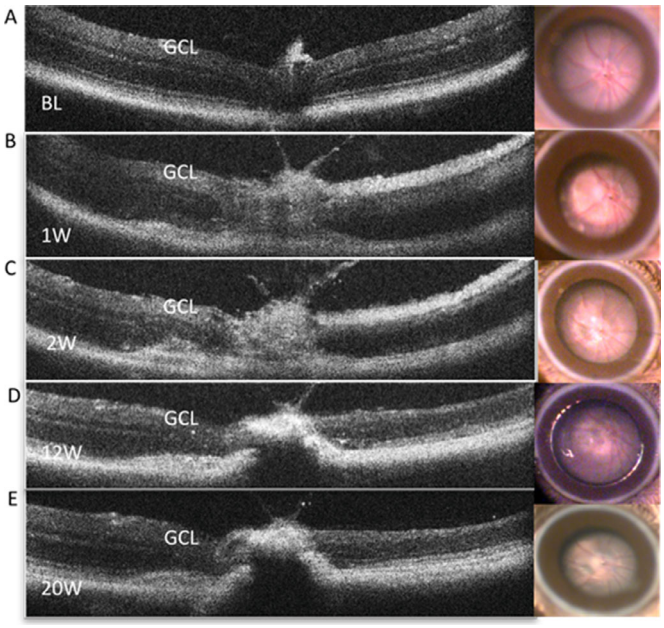

Figure 1. OCT and fundus images before and after mice receiving Nd:YAG laser. (A) Baseline image, (B) One week after laser and (C) Two weeks after laser. We can observe retinal edema and subretinal fluid in the right part where laser treated at one week after laser and this phenomenon disappear around two weeks after injury. (D) Twelve weeks after laser and (E) 20 weeks after laser show the thinning of GCL and IPL.

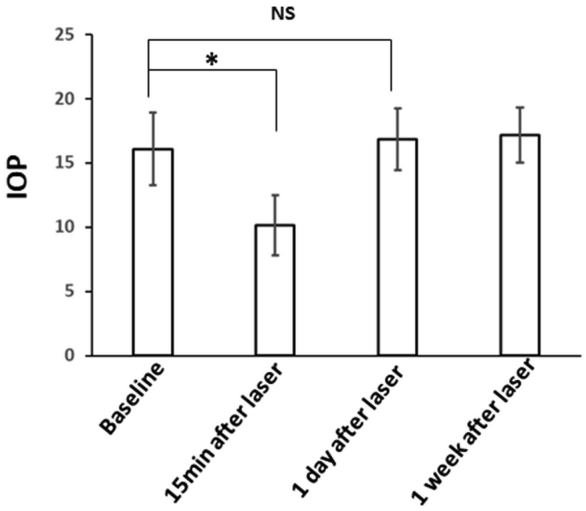

Figure 2. IOP measurements before and after the injury. Nd:YAG laser induces a temporal IOP decrease after treatment. However, the IOP returns to normal level soon one day after injury. There is no statistically difference between IOP measured at baseline and one day after laser. The IOP remains stable from one day after injury.

Compared with the baseline IOP (16.1 ± 2.85 mm Hg), the IOP decreased 15 minutes after the laser injury

Table. Nd:YAG Laser Does Not Produce Severe Side Effects

Side Effects	Occurrence Rate (%)	Lasting Days
Corneal edema	49	3
Corneal neovascularization	0	/
Corneal calcification	0	/
Cataract	0	/
Vitreous hemorrhage	18	14
Mortality	0	/

(10.1 ± 2.33 mm Hg, $P < 0.01$). However, the IOP returned to normal level at one day after injury and no statistical difference existed between baseline IOP and the IOP measured one days after laser treatment (16.9 ± 2.41 mm Hg, $P = 0.45$). Since then, the IOP remained stable (17.2 ± 2.14, $P = 0.36$) (Fig. 2).

Corneal edema occurred in 49% (22/45) of the mice after laser (most likely from the use of a coverslip over the cornea during the laser procedure)—all of which disappeared within three days. Corneal neovascularization and corneal calcification were not observed in any mice. Cataract or other anterior chamber pathology was not detected after the laser injury; however, 16% of the mice (7/45) developed cataract by the end of each imaging experiments—likely a result of the repeated in vivo imaging process longitudinally. Typically, these metabolic cataracts disappeared within three days after laser treatment and each imaging experiment. In 18% (8/45) of the mice, the photodisruptive Nd:YAG laser blast hit a main vessel and caused a small amount of vitreous hemorrhage, all of which was absorbed within two weeks. We quantified the RGC number at the end of the experiment and did not observe any significant difference between these eight mice and the other 37 mice. The Nd:YAG laser injury did not result in any mortality. All mice recovered from the TON procedure, and no intraocular inflammation was observed (Table). We also did not observe any significant body weight difference between mice with ND:YAG laser

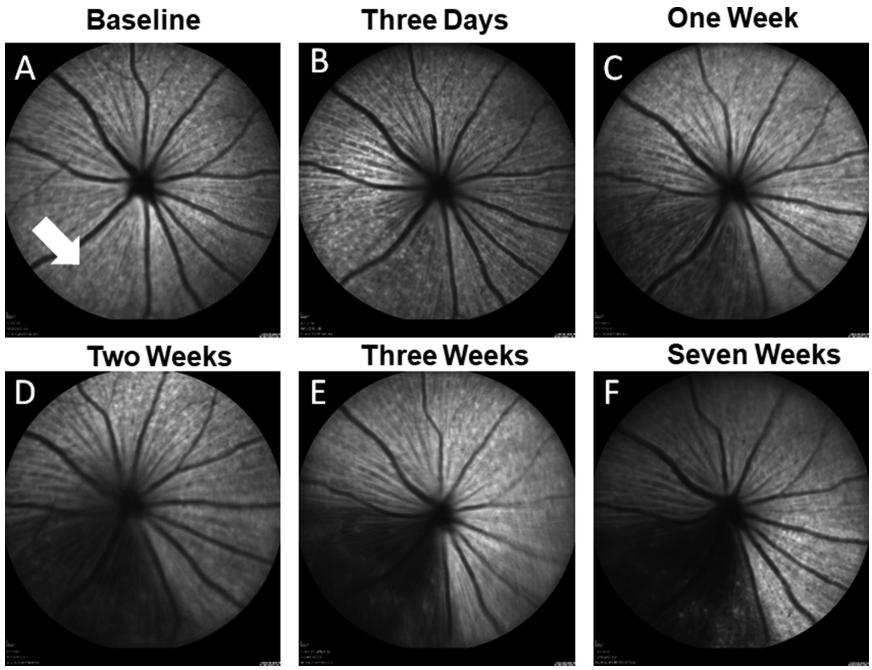

Figure 3. Confocal laser scanning ophthalmoscope images of mice before and after receiving Nd:YAG laser treatment. (A) Baseline image. The Nd:YAG laser spot is shown by the *white arrow*. (B) One week after laser, inferotemporal retina starts to lose fluorescence. Lasered area progressively losses Thy-1 RGC at (C) one week, (D) two weeks, (E) three weeks, and (F) seven weeks after crush.

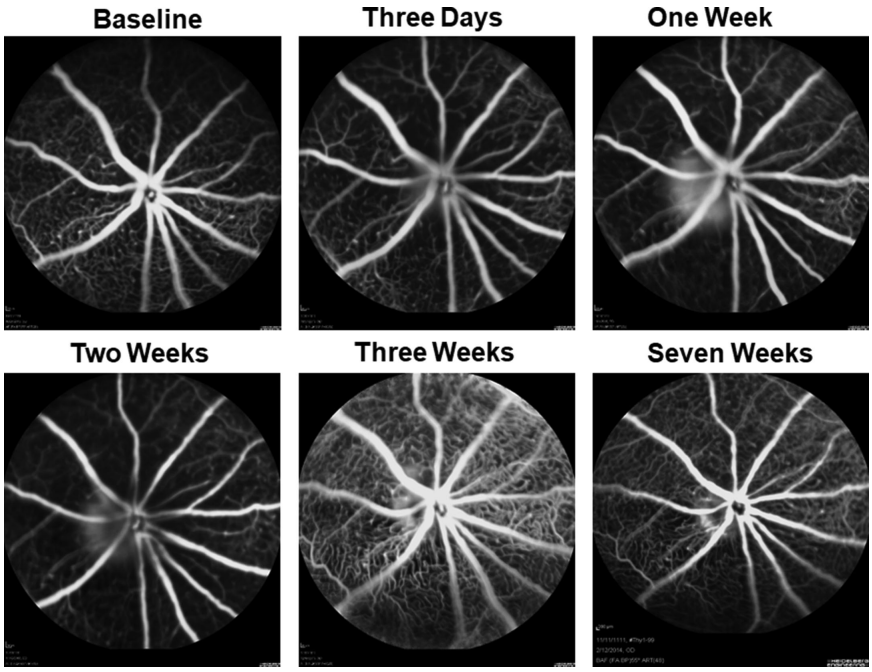

Figure 4. Fundus fluorescein angiography (FFA) images of mouse retina before and after Nd:YAG laser treatment. The FFA showed similar levels of fluorescence in the vessels of the affected and unaffected areas, indicating the hypofluorescence was caused by the loss of RGCs, rather than obstructions.

treatment and mice without laser treatment (Supplementary Fig. S1).

ND-YAG Laser Induces RGC Death in the Localized Injury Area

We can observe the whole retina is brightly lit by CSLO at baseline because of the presence of GFP-labeled retinal ganglion cells. Functional RGC express eYFP in both the soma and axon, appearing as bright hyperfluorescent spots in the retinal images. On the other hand, apoptotic or necrotic RGCs express no fluorescence, are typically not visible with CSLO imaging, and appear as a dark background. One week after the focal Nd:YAG laser injury to the retina, CSLO imaging shows localized hypofluorescence in the laser area, indicating the loss of Thy-1 RGCs in the laser area. We observe this pattern 20 weeks after retinal laser injury, while non-lasered area remain stable with normal fluorescence signal intensity and density (Fig. 3). FA showed similar levels of fluorescence in the vessels of the affected and unaffected areas, indicating the hypo-fluorescence was caused by the loss of RGCs, rather than obstruction of the confocal imaging by vitreous hemorrhage (which was not visible by direct viewing) or retinal hemorrhage (Fig. 4).

Immunofluorescence images of retina wholemounts also show the loss of RGCs in the laser region. Compared with the non-injured region in the same retina, RGC density was significantly lower in laser injured regions. The number of GFP positive thy-1 RGC and brn3 (an RGC specific cell marker) expressing cells were significantly decreased (Figs. 5A, 5D, 5G, 5K). Furthermore, the axons of RGCs in these regions were much thinner less compared to those in non-laser regions (Figs. 5G–5I).

ND:YAG Laser Causes RNFL Loss in the Lasered Area

Compared with the baseline OCT image, the retinal thickness heat maps show a significant thinning of the RNFL in 25-35% of the retina in the region directly within the photodisruptive laser blast radius, centered on the main targeted site of laser energy delivery (Figs. 6A–D). The RNFL of the injured retina attenuated with the time (Fig. 6E). The RNFL of the study eyes was significantly thinner than that of the control eyes two weeks after photodisruptive laser injury. Confirming the retinal nerve fiber loss, the pattern of RNFL thinning matches the pattern and amount of fluorescence loss on CSLO images which is a measure of RGC density. (Figs. 6A–D)

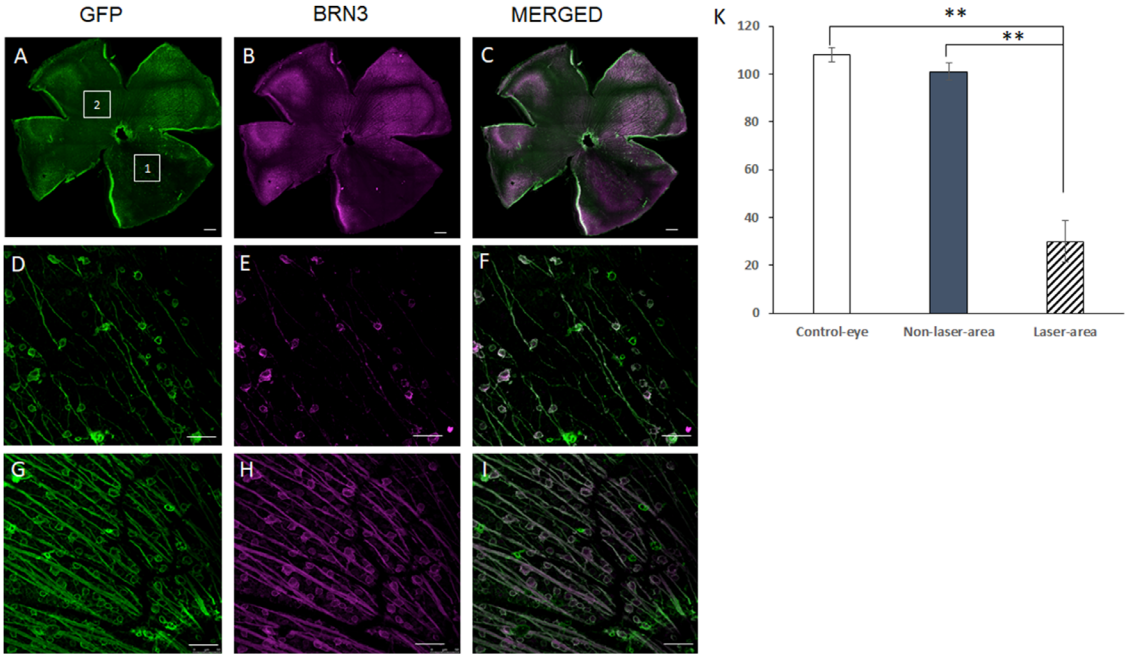

Figure 5. Retinal wholemount images of mouse after Nd:YAG laser treatment. (A-C) Whole retina images show characteristics of GFP-positive Thy-1 retinal ganglion cells and BRN3 positive retinal ganglion cells (RGCs). (D, E) Amplified images from area 1, which is laser treated area. Numbers of GFP positive and Brn3 positive cells are significantly decreased. (G–I) Amplified images from non-laser-treated area 2. *Scale bar*: 50 µm. (K) The RGC number counting results in contralateral eye, non-laser-area in lasered eye and laser-area in lasered eye. The counting is based on the positive Brn3 staining.

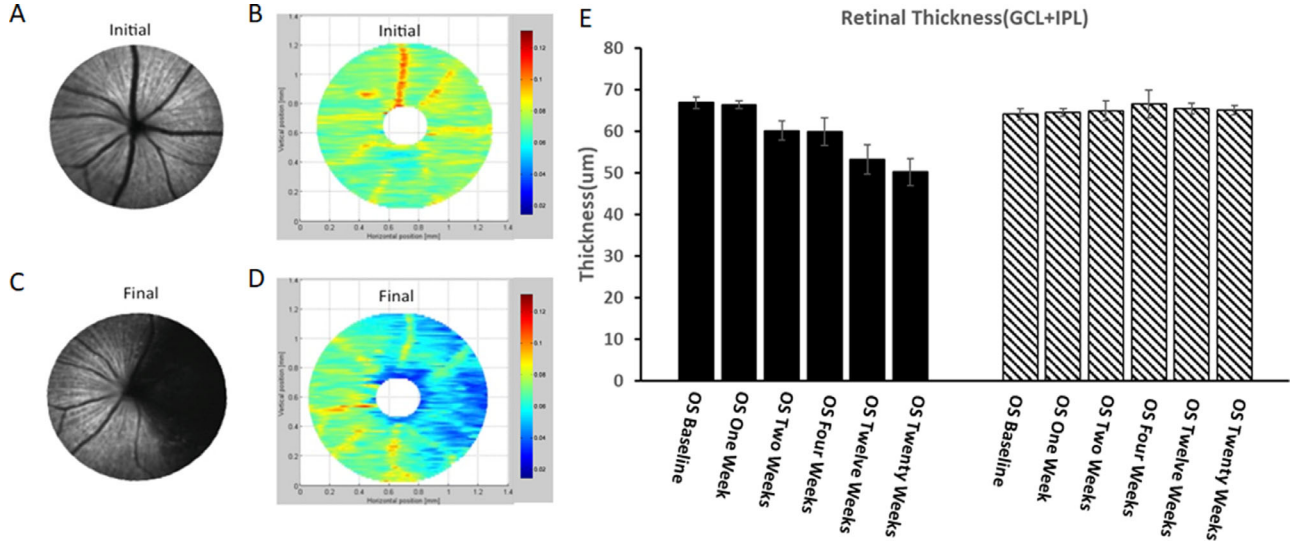

Figure 6. The thickness of nerve fiber layer decreased after ND:YAG laser treatment. (A) CSLO image of retina before the laser. (B) OCT thickness heat map of mouse retina before laser. (C) CSLO image of retina four weeks after the laser. (D) OCT thickness heat map of mouse retina four weeks after laser. The pattern of RNFL thinning matches the pattern of fluorescence loss on CSLO images. (E) Quantification results of nerve fiber layer thickness.

Based on analysis of the heat maps and CSLO images, no change occurred in areas outside of the laser radius in experimental retinas. This suggests a high proportion of RGCs within the blast range were disrupted and ablated by the Nd:YAG laser, while the retina outside of the range was largely unaffected. The thinning of the RNFL and loss of RGCs were also confirmed by *in vitro* histopathology and immunohistochemistry. Hematoxylin-eosin staining showed that compared with the control eye, the RGC layer was

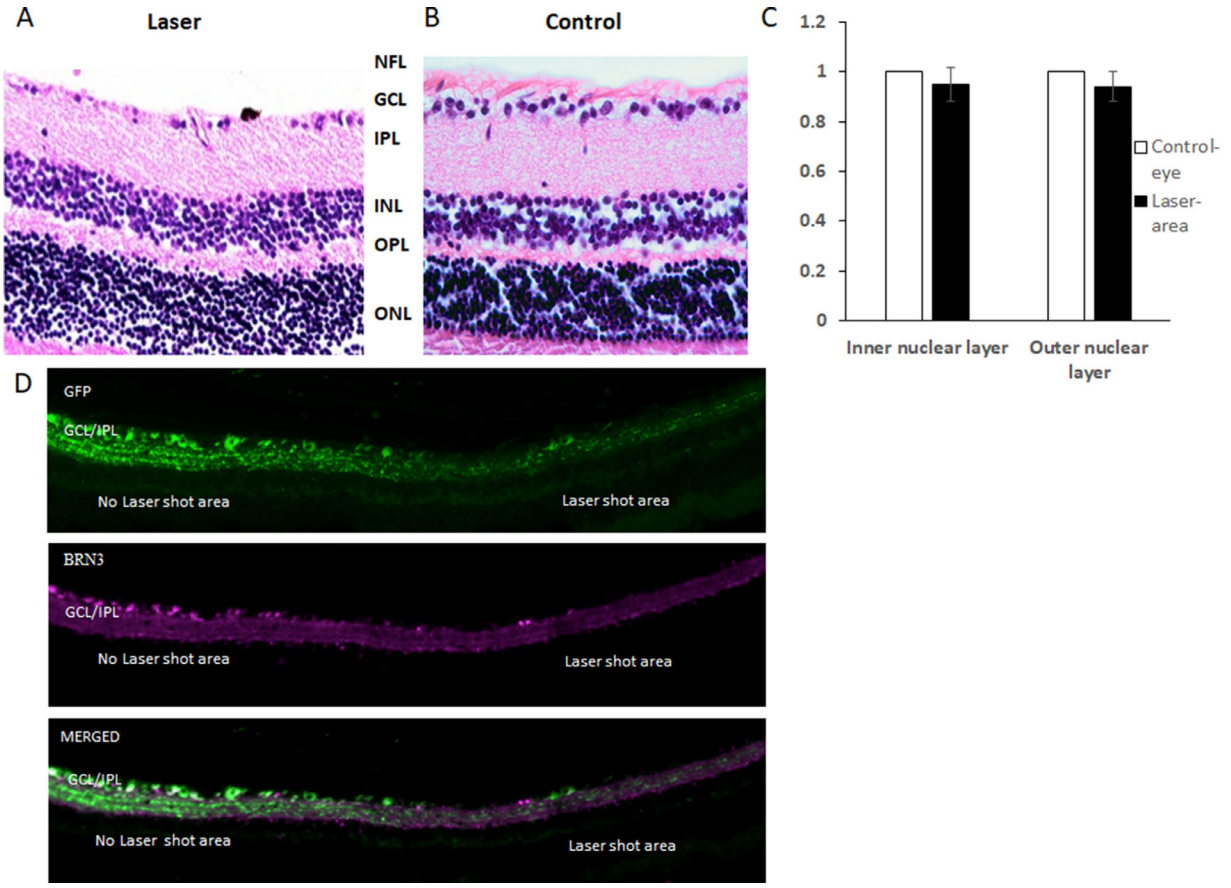

Figure 7. Nd:YAG laser causes nerve fiber layer loss and RGC death. (A) Hematoxylin and eosin (H&E) staining of laser-treated retina four weeks after injury. (B) H&E staining of non-laser control retina. (C) Cell counting results. The nuclear number of inner nuclear layer and outer nuclear in laser eyes are compared to control eyes. (D) Immunostaining of laser-treated and non-laser control retinas. We could observe the decreased number of GFP and BRN3 positive RGCs in lasered area.

significantly thinner with far fewer RGCs in the laser injured area of the study eye, while the RNFL was entirely disrupted. No significant structural difference was observed beneath the GCL layer between study and control eyes. (Figs. 7A–B). There is no significant difference between the nuclear number in inner nuclear layer and outer nuclear layer in lasered eyes and control eyes (Fig. 7C). Immunofluorescence staining of the cross-sectional samples further demonstrate the thinning of nerve fiber layer, ganglion cell layer and inner plexiform layer along with significantly decreased number of RGCs, labeled with GFP and BRN3a in the laser-injured area (Fig. 7D).

RGC Function is Decreased in Nd:YAG Laser Model

To study whether ND:YAG laser affects RGC function in association with loss of RGCs due to Nd:YAG laser ablation, pattern ERG (PERG) recordings were obtained at baseline, one week, one month and two months after laser treatment. PERG is designed to specifically measure RGC function. PERG amplitudes in treated eyes continuously decreased over time and were lower than with non-laser treated control eyes. The amplitude difference between baseline and one week and one-month time points are not significant, but the difference between baseline and two-month time point is significant. The average PERG amplitude of treated eyes at two months after laser treatment is 14.99 μV, significantly lower than 25.29 μV at baseline and 23.25 μV in the contralateral eyes (Fig. 8A). A statistically significant increase in the PERG peak latency of laser-treated eyes was also observed (Fig. 8B). The representative PERG results were plotted for the lasered-treated eyes and control eyes two months after injury (Fig. 8C). Compared to control eyes, the peak is blunter, and the waveform is shifted to the right in the laser-treated eye. These data suggest the ND:YAG laser induces a progressive and consistent loss of RGC function longitudinally

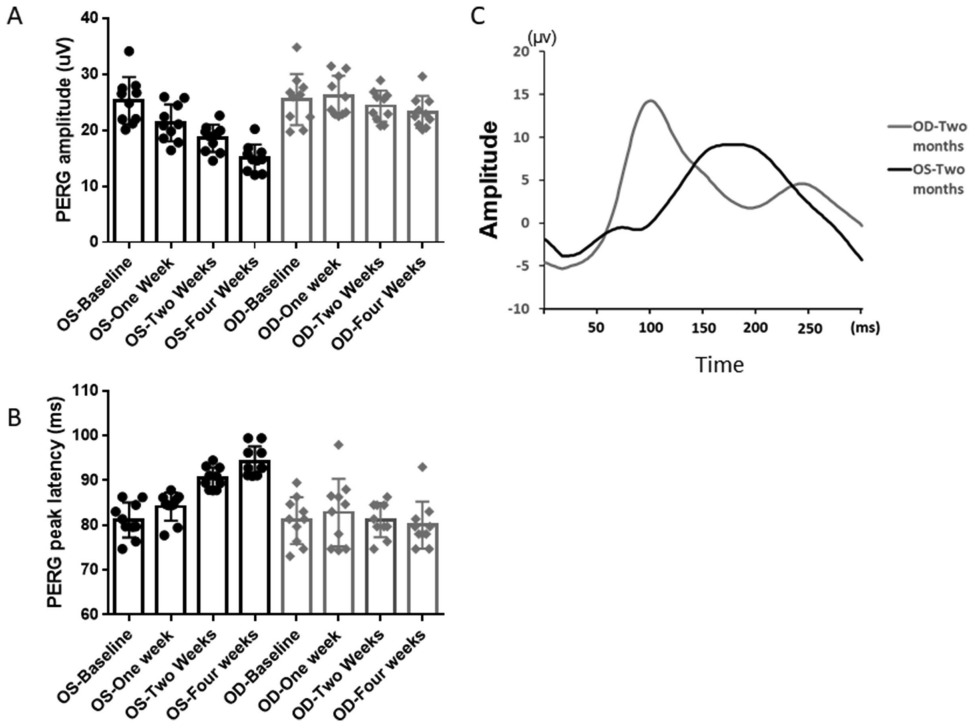

Figure 8. RGC function decreases after Nd:YAG laser treatment. PERGs were recorded at baseline, one week, one month, and two months after laser. The PERG amplitude (A) and PERG peak latency (B) at baseline, one week, one month, and two months after laser were compared in the treated (OS) and contralateral eye (OD). (C) Representative PERG results were plotted for the treated and control eyes two months after laser.

consistent with RGC loss over time as measure by OCT and CSLO.

Discussion

We present a new model of traumatic neuropathy using a photodisruptive Nd:YAG laser to create a cloud of energy to directly deliver a site-specific and titratable reproducible retinal injury. To our knowledge, there has been no publication of a similar model previously. This photodisruptive laser traumatic optic neuropathy model possesses many advantages, especially relative to other currently used models as mentioned above. Nd:YAG photodisruptive laser-induced trauma is reproducible, the injury can be followed longitudinally in vivo, and the damage is limited to the eye with no mortality. Most importantly, the magnitude of concussive laser injury can be precisely adjusted by titrating the amount of laser energy delivered to the eye, and the injury region can be controlled by precisely determining the placement and location of the laser beam used to induce laser trauma within the eye. This is a significant advance in comparison to the more diffuse ocular damage seen in many of the published traumatic optic neuropathy models, especially those associated with closed chamber blunt ocular damage.

To date, most models for neuropathy involve direct blunt force trauma to the globe, for example, concussive models. Concussive models are those that use direct compressive force onto the eye—this is the approach used by the studies by Linlin Zhang[9] and Tania Rex.[7] One used the pendulum to smash the eye and the other an air gun. Although these models accurately recreate the most common mechanism of severe injury, they are often associated with side effects that are not often observed in human eye injury. These side effects include systemic inflammation, changes in IOP, corneal edema, and calcification. The Rex model even reports mortality up to 20%.[8] However, our model of TON using a photodisruptive force generated by a YAG laser intraocularly did not cause any animal death. This model directs trauma directly to the peripapillary region where the laser energy is placed and does not cause concussive shear force throughout the globe, which leads to generalized ocular trauma, including transmitted force to the brain and head. Our model is a signifi-

cant improvement from these models, in that very few side effects are observed. The main side effects seen in our study were corneal edema, vitreous hemorrhage, and cataracts, which were all transient and reversible. The first two of these were temporary, resolving within the first three weeks after injury. Cataract formation was seen in 16% of the mice in our trial. However, because the cataracts formed weeks after the laser injury, the cataracts most likely were caused by the ocular trauma of repeated in vivo imaging, rather than being a direct result of laser injury, because we also observed similar cataracts in the non-laser-treated eyes. No significant difference in IOP between experimental and control eyes, or between baseline measurements and measurements at one and seven days after injury was observed. No persistent intraocular inflammation or mortality was observed in our mice.

The YAG laser works by photodisruption with atomization of tissue but also with a microexplosion with a photodisruptive concussive shockwave of force that not only ablates tissue but also produces a pulsatile energy cloud.[16] When the Nd:YAG laser focuses on a small spot, the ND:YAG laser can deliver calibrated, discrete laser pulses in very short time periods with tunable fixed power that is reproducibly controlled by the laser operator spatially and temporally. When the Nd:YAG laser beam focuses above the retina, it can cause injury that simulates blast trauma through the generation of a concussive shockwave. In contrast, when the laser is focused on tissue, the tissue is ablated by photodisruption and atomized. The main advantage of using an Nd:YAG laser to create a retinal injury is that the laser can focus directly on a targeted region with precise control, thereby allowing for a consistent and measured amount of damage to tissue compared to other existing models of ocular trauma that are diffuse and nonspecific to particular ocular structures. Therefore some of the more commonly used blast injury models such as using a paint gun can result in animal death or systemic injury or effects.[7,17]

The damaged retinal area observed on CSLO was larger than the laser spot diameter. The Nd:YAG laser induces shockwave damage like a concussive bomb force that not only damages the direct area of laser delivery but also the nearby retina, which is impacted by the cloud of concussive Nd:YAG laser photodisruption. Compared to other traumatic retinal damage models, the retinal injury in our model is specific to RGCs without causing damage to other retina layers when the laser energy cloud is de-focused onto a spot above the retina. With OCT imaging, the GCL becomes thinner longitudinally, and the OCT NFL density heatmap shares a similar overlying injury pattern as in CSLO images, which assess RGC density and spatial location. We also observed the ND:YAG laser–induced RGC loss was accompanied by RGC functional loss as measured by pattern ERG amplitude and latencies. The flash ERG and other histological analysis further confirmed that the outer retina function is not affected by the laser.

Another advantage of using a Nd:YAG laser to create retinal injury in an optic nerve injury animal model is that the location and degree of injury are highly controllable. When the laser is focused directly on tissue, the tissue is ablated by photodisruption and atomized. In contrast, when it is focused above the retina, it can cause injury that simulates blast trauma through the generation of a concussive shockwave force from the Nd:YAG laser. This laser technique is easy to perform, reproducible, and results in an injury that can be focused to any desired spatial area of the retina. Furthermore, the intensity of the blast can be titrated by increasing the laser energy. Although our study found that in mice, a laser energy of higher than 0.4 mJ resulted in vitreous hemorrhage, a higher energy may be warranted for other animal models or for different types of injury.

In summary, we have created a new and novel RGC death model that confers no mortality when performed correctly and produces a quantifiable decrease in RGC number and function. This injury model is simple to implement and is reproducible. The laser causes primary RGC death in the lasered area while inducing secondary degeneration in the surrounding area. We believe this new model addresses the shortcomings of previous animal models and has potential application in the study of RGC protection and axon regeneration. This model can also be a powerful tool in developing and identifying new treatment modalities for traumatic ocular injury.

Acknowledgments

Supported by NIH Center Core Grant P30EY014801, a Research to Prevent Blindness Unrestricted Grant, the Camiener Family Glaucoma Research Fund, and the Gutierrez Family Research Fund. R.K. Lee is supported by the Walter G. Ross Foundation.

Disclosure: **X. Xing,** None; **X. Tong,** None; **Y. Liu,** None; **M. Tapia,** None; **P. Jin,** None; **T.D. Holley,** None; **O. Qiu,** None; **R.K. Lee,** None

* XX and XT contributed equally to this work.

References

1. Blanch RJ, Good PA, Shah P, Bishop JR, Logan A, Scott RA. Visual outcomes after blunt ocular trauma. *Ophthalmology*. 2013;120:1588–1591.
2. Lee V, Ford RL, Xing W, Bunce C, Foot B. Surveillance of traumatic optic neuropathy in the UK. *Eye (Lond)*. 2010;24:240–250.
3. Pirouzmand F. Epidemiological trends of traumatic optic nerve injuries in the largest Canadian adult trauma center. *J Craniofac Surg*. 2012;23:516–520.
4. Weichel ED, Colyer MH, Ludlow SE, Bower KS, Eiseman AS. Combat ocular trauma visual outcomes during operations Iraqi and enduring freedom. *Ophthalmology*. 2008;115:2235–2245.
5. Lee R, Sayed M. Anterior Segment Trauma. In: Yan H, ed. *Mechanical Ocular Trauma*. Singapore: Springer; 2017;7–38.
6. Gregor Z, Ryan SJ. Combined posterior contusion and penetrating injury in the pig eye. III. A controlled treatment trial of vitrectomy. *Br J Ophthalmol*. 1983;67:282–285.
7. Hines-Beard J, Marchetta J, Gordon S, Chaum E, Geisert EE, Rex TS. A mouse model of ocular blast injury that induces closed globe anterior and posterior pole damage. *Exp Eye Res*. 2012;99:63–70.
8. Mohan K, Kecova H, Hernandez-Merino E, Kardon RH, Harper MM. Retinal ganglion cell damage in an experimental rodent model of blast-mediated traumatic brain injury. *Invest Ophthalmol Vis Sci*. 2013;54:3440–3450.
9. Yan H, Li F, Zhang L. A new and reliable animal model for optic nerve injury. *Curr Eye Res*. 2012;37:941–948.
10. Tao W, Dvoriantchikova G, Tse BC, et al. A novel mouse model of traumatic optic neuropathy using external ultrasound energy to achieve focal, indirect optic nerve injury. *Sci Rep*. 2017;7:11779–017.
11. Jones NP, Hayward JM, Khaw PT, Claoue CM, Elkington AR. Function of an ophthalmic "accident and emergency" department: results of a six month survey. *Br Med J (Clin Res Ed)*. 1986;292:188–190.
12. Schuman JS, Hee MR, Puliafito CA, et al. Quantification of nerve fiber layer thickness in normal and glaucomatous eyes using optical coherence tomography. *Arch Ophthalmol*. 1995;113:586–596.
13. Wu H, de Boer JF, Chen TC. Reproducibility of retinal nerve fiber layer thickness measurements using spectral domain optical coherence tomography. *J Glaucoma*. 2011;20:470–476.
14. Munguba GC, Galeb S, Liu Y, et al. Nerve fiber layer thinning lags retinal ganglion cell density following crush axonopathy. *Invest Ophthalmol Vis Sci*. 2014;55:6505–6513.
15. Camp AS, Ruggeri M, Munguba GC, et al. Structural correlation between the nerve fiber layer and retinal ganglion cell loss in mice with targeted disruption of the Brn3b gene. *Invest Ophthalmol Vis Sci*. 2011;52:5226–5232.
16. Chou TH, Bohorquez J, Toft-Nielsen J, Ozdamar O, Porciatti V. Robust mouse pattern electroretinograms derived simultaneously from each eye using a common snout electrode. *Invest Ophthalmol Vis Sci*. 2014;55:2469–2475.
17. Vogel A, Capon MR, Asiyo-Vogel MN, Birngruber R. Intraocular photodisruption with picosecond and nanosecond laser pulses: tissue effects in cornea, lens, and retina. *Invest Ophthalmol Vis Sci*. 1994;35:3032–3044